Vol. 1, No. 1, pp. 75-109, (December 2023)

ASWAN SCIENCE AND TECHNOLOGY BULLETIN (ASTB)

Online ISSN: 3009-7916, Print ISSN: 1110-0184

Journal homepage: https://astb.journals.ekb.eg/ E-mail: essamshaalan@sci.aswu.edu.eg

Original Article

Optical Characterization of Ge30-xSbxTe10Se60(0 ≤ x ≤ 20) Thin Films for Optoelectronics.

N. N. Ali Karrar[1,2], A. A. Elamin[2], Fouad Abdel-Wahab[2], M. M. Soraya[2*]

[1)]Egyptian Environmental Affairs Agency, Aswan, Egypt

[2)]Physics Department, Faculty of Science, Aswan University, Aswan, Egypt

Received: 02/10/2023 Accepted: 03/12/2023

Abstract:

The quenching procedure has been utilized for the preparation of the bulk of chalcogenide glasses Ge_{30-x} Sb_xTe_{10} Se_{60} where mass% (x =0, 5, 10, 15, 20), the samples were made into thin films using the thermal evaporation method. The optical characterization of the films was performed using a two-beam spectrophotometer with a 400–2500 nm wavelength range. The refractive index n was deduced, it showed that n increased with increasing Sb concentration. The optical band gap E_g was observed to decrease as Antimony concentration increased, where E_g falls from 1.375 to 1.009 eV. This decrease in E_g is described by the average single bond energy, Urbach energy, where the average single bond energy falls from 23.55to 19.87 Kcal g^{-1} at^{-1} as Sb content increases, and Urbach energy rises from 0.29 to 0.4 eV as Sb content increases. For all the samples, raising incoming photon wavelength causes the real and imaginary components of the dielectric constant diminish., whereas increase with increasing Sb doping rate. Wemple and DiDomenico dispersion model was utilized to calculate the dispersion parameters for incontent.e single-oscillator energy E0, the dispersion energy Ed, and the static refractive index no; it was found that the values of E0 roughly match the energy gap's twofold value, and the values of E_d and E_0 fall as the antimony content rises , where Ed value falls from 26.47 eV to 20.19 eV , and the value of E_0 falls from 3.89 to 2.62 eV while no increase from 2.796 to 3.022 with increasing Antimony content . The loss factor's estimated values demonstrate an increase as photon energy rises, as well as an increase in antimony content. An increase in non-linear refractive index n_2 as antimony concentration increases where n_2 rises from $1.99x10^{-10}$ to $3.73x10^{-10}$ esu. Their entire potential for nonlinear optics may be found in the mid-infrared region due to their low optical band gap energy. These materials

have wide IR transparency and high (non)linear refractive indices, which make them desirable for optical nonlinear devices.

Keywords: $Ge_{30-x}Sb_xTe_{10}Se_{60}$, thin films, Optical properties, nonlinear refractive index, IR Sensors

1. Introduction

Glasses with chalcogenide metal doping are now a crucial subset of the non-crystalline semiconductor market. These materials can be vital in the field of optical electronics **(Giri *et al*., 2023)** owing to the excellent transmission in the near and far IR spectral range **(Wang *et al*., 2011)** . Due to their novel and distinguishing characteristics, such as their high linear and non-linear refractive indices, outstanding transmittance range, larger band gap, low phonon energy, etc., these alloys are in great demand (**Kumar & Dwivedi,2013; Lee *et al*., 2018)**. As a result, they are widely used in devices such as holography, waveguides, LEDs, IR sensors (**Halenkovič *et al*., 2022)** , and photo detectors**.(Hassanien & Akl,2016; Hassanien & Akl,2016)** ,have a high refractive index and 102 times more nonlinearity than silica, respectively **(Sharma *et al*., 2011)**, and they serve switching devices **(Eggleton *et al*., 2011; Behera *et al*., 2017).**

Optical electronics application with chalcogenide materials is straightforward due to the stability of their chemical and thermal properties **(Fayek *et al*., 2001; Désévédavy *et al*., 2010; Jung *et al*., 2017; Hassanien &Akl,2018; Mishra *et al*., 2019)**.Addition of metals in a matrix alters the average coordination number and accordingly compositional modifications **(El-Metwally *et al*., 2022)** , such that the network becomes flexible, intermediate, or rigid. As a result, controlled changes to physical and optical characteristics may be made to meet industry requirements **(Sharma *et al*., 2017; Abbady & Abd-Elnaiem,2019)**. Historically, pure Se has been chosen to be the host matrixes for chalcogenides, due to its excellent capacity to form glass **(Mott & Davis,1979)**. However, Se in its pure form has certain drawbacks, including a limited sensitivity and a short lifetime. Se has been alloyed with a select few favored additives to get around these limitations **(Vashist *et al*., 1953; Mott & Davis,1979; Sharma *et al*., 2008)**.

Corresponding author*: E-mail address: somahmoud_81@yahoo.com

Te in its pure form has a low capacity to form glass, however despite this drawback, it exhibits outstanding non-linear characteristics, transparency in IR, a high *n*, and change in the phase. the chalcogenide which based on Se and Te has been used as the primary host matrix in this inquiry because of its modified characteristics, which include relatively high sensitivity to light, hardness, beneficial influence on ageing, and a higher temperature of crystallization. **(Shimakawa,1985; Chauhan *et al.*, 2010)**. The application realm may be expanded by the inclusion of a third component, which can improve the Se-Te binary composition. As the third network element, Ge is chosen. in the current study. Ge greatly improves the area where glass forms, and thermal stability, and reduces the impacts of ageing as crosslinking is produced by Ge using Se chains, thereby boosting the system's average bonds and acting as a bond modulator. Ge even produces a very stable glassy melt when its size and electronegativity levels are compatible **(Shimakawa,1985; Sharma *et al.*, 2008)**. Many studies have investigated how Sb influences the optical characteristics of Ge-Se chalcogenide ternary thin films. **(Abdel-Wahab *et al.*, 2013; Abdel-Wahab *et al.*, 2017; Abdel-Wahab *et al.*, 2020).,** and the thermal characteristics of quaternary Ge- Sb-Se-Te **(Soraya *et al.*, 2023)**. The electrical, optical, structural, physical, and thermal characteristics of diverse ternary and quaternary systemshave been examined in previous publications. **(El-Ocker *et al.*, 1998; Akl & Hassanien,2015; Hassanien *et al.*, 2016; Hassanien *et al*, 2016; Kumar *et al.*, 2017; Hassanien & Akl,2018; Kumar *et al.*, 2018)** ,and come up with results having a wide range of possible industrial applications.

The present work's goal is to examine the influence of addition of Sb in the Ge-Se-Te network. In earlier research **(Hassanien & Sharma,2019; Hassanien & Sharma,2020)**. optical and a few physical characteristics of the Ge-Se-Sb-Te amorphous samples were examined. With Ge replacement by Sb, new defects are being formed in the network, according to changes in optical and physical factors. As a result, it has an influence on the films' short- and medium-range planning, which further leads to the customization of the assets. Addition Bi and Sb facilitate reversible of the carrier type in the matrix and unpin Fermi level, which expands the network's glassy area, improves the stability of the thermal properties, and boosts transmission in IR spectral range. Sb-doped **Ge-Se-Te** glasses are an outstanding multifunctional material with a variety of applications**(Chen *et al.*, 2018; Fouad *et al.*, 2018; Yoo *et al.*, 2018)**A modification in the chemical composition's structures is anticipated because Sb is utilized as a chemical modifier and also produces compositional and configurational disorders **(Chen *et al.*, 2018; Fouad *et al.*, 2018)**.Recent research has shown that the Sb-addition enhances the

thermal characteristics of the host lattice of **Ge-Se-Te**, which accordingly increases *n* values**(Hassanien & Sharma,2019; Hassanien & sharma,2020)**. Besides this, several optical properties were carried out due to its offer own features and significant benefits. Therefore, the current paper seeks to understand and explain certain crucial physical and optical factors of Ge_{30-x} Sb_xTe_{10} Se_{60} where mass% (x =0, 5, 10, 15, 20) glassy samples and to investigate the correlations between the features of GSST network and its corresponding films. From the perspective of applications. The influence of replacing Ge by Sb in the network of **Ge-Sb-Se-Te** on the optical and physical characteristics of Ge_{30-x} Sb_xTe_{10} Se_{60} are investigated and discussed. Therefore, researching a material's optical constants is crucial to determining the material's possible opto-electronic applications **(Dongol,2002)**. Additionally, the atomic structure, electrical characteristics, and electronic band structure of the material may all be strongly connected to the optical qualities. On thin film samples, the optical constants may be precisely measured with ease. To choose which materials to use in optoelectronic devices, it is crucial to consider their optical behavior **(Pandey *et al*., 2005)**. The band gap has a significant impact on semiconductors' electrical characteristics **(Beyer et al., 1971; Sati et al., 2006).**

2. The Materials and Methods

2.1 Bulk materials Preparation

The melt-quench technique is the method to generate the bulk of the (Ge_{30-x} Sb_xTe_{10} Se_{60}) where (X=0, 5, 10, 15, 20). Adequate quantities of pure Germanium (99.9999%), antimony, tellurium, and selenium were accurately weighted by Shimadzu AW220 electrical balance. Silica ampoules that were 1.5 cm in diameter and 20 length cm were first, cleaned after being submerged in chromic acid for 24 hours, rinsed in deionized water, then dried at 60 ^{o}C in a drier furnace, finally, the weighted ingredients were put into long these tubes. By using an oil diffusion pump, the tubes were securely sealed in a vacuum of approximately 10^{-5} torr to prevent oxygen contamination. Each ampoule was heated individually in an electrical muffle furnace at a heating rate of 3°C to 4°C/minute after the components had been mixed in the ampoules. For nine hours, the temperature increased to 1000 °C. To maintain the compositions' homogeneity, the ampoules were often shaken. The ampoules were then secured in a horizontal position while the molten substance was quickly cooled in ice-water. After cooling, the silica ampoules were broken to free the ingots from the tubes, and they were then maintained at ambient temperature in a dry environment.

2.2 Thin films Preparation

Glass substrates were washed by acetone on ultrasonic followed by distilled water, and at 60 °C were dried by dryer furnace. The most used technique for creating thin films is thermal evaporation. This was accomplished using the coating system (Denton Vacuum DV 502 A, Cherry Hill, NJ, USA). The weighted ingredients were put into a resistive vessel consisting of metals with a high melting point and linked to an external source of strong electric current, the thin film samples were applied to the clean glass substrates using the vacuum thermal evaporation process. To keep track of the created films' thickness throughout the evaporation process; thickness monitor (FTM6) was used, and the thickness are mostly greater than 1000 nm, the substrates were maintained at 300 K room temperature throughout the deposition procedure, with the deposition rate being set at 2 nm/sec. To produce a uniform and smooth film, the substrates were rotated at a modest speed of 5 Rev/min. A two-beam spectrophotometer (UV-VIS-NIR JASCO-670) with a computerized data collecting system was used to test the optical absorption and transmission of thin film samples in the UV and visible range. The measurements were made in the 400 to 2500 nm wavelength range, with normal incidence at room temperature.

2.3 Materials Characterization

The energy dispersive X-ray spectroscopy (EDXS) is technology that provides accurate information on the fundamental components of alloys. The scanning electron microscopy (SEM) is useful in the examination of the structure and the observation of the morphological change of the thin film. scanning electron, the samples were examined utilizing (JOEL-JSEM-T200) scanning electron microscope. The amorphous character of the glasses was determined by an X-ray diffraction system that is completely computerized (Shimadzu Lab XRD 6000) using filtered copper radiation, ⌊=1.54060A,the pattern was recorded at a scanning rate of 20/min.

3. Results and Discussion

3.1 Structural Characterization

The compositions of the prepared samples were investigated by the energy dispersive spectral (EDS). The spectral distribution of the constitute elements of the samples were determined using EDS as shown in **Fig.1 (a-e)**, the compositions of the **Ge-Sb-Se-Te** were determined using EDXS, the ratio of atomic % of Ge, Sb,Te and Se were shown in Table1. A

small deviation was found between the theoretical calculated compositions and those listed in **Table1**, and **Fig.1** illustrates the elemental composition by EDXS quantification confirms that there are no impurity elements in the current samples. XRD was utilized to confirm the amorphous nature of the prepared samples were confirmed by as shown in **Fig.2** SEM micrographs show the absence of crystallization phase in the micrograph and is homogeneous in nature., which is evident from the SEM images displayed in **Fig.3(a-e).**

Fig. 1a

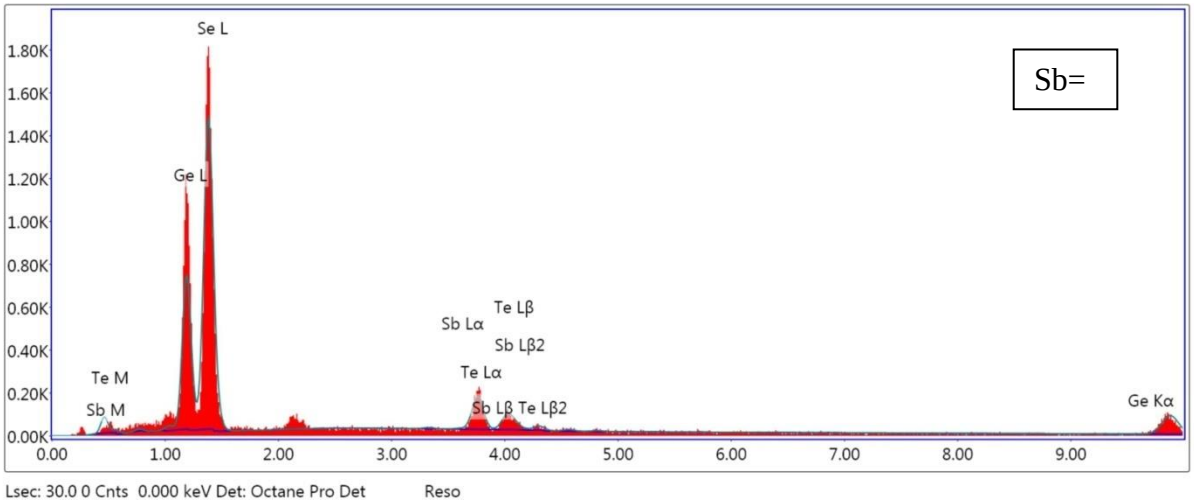

Fig. 1b

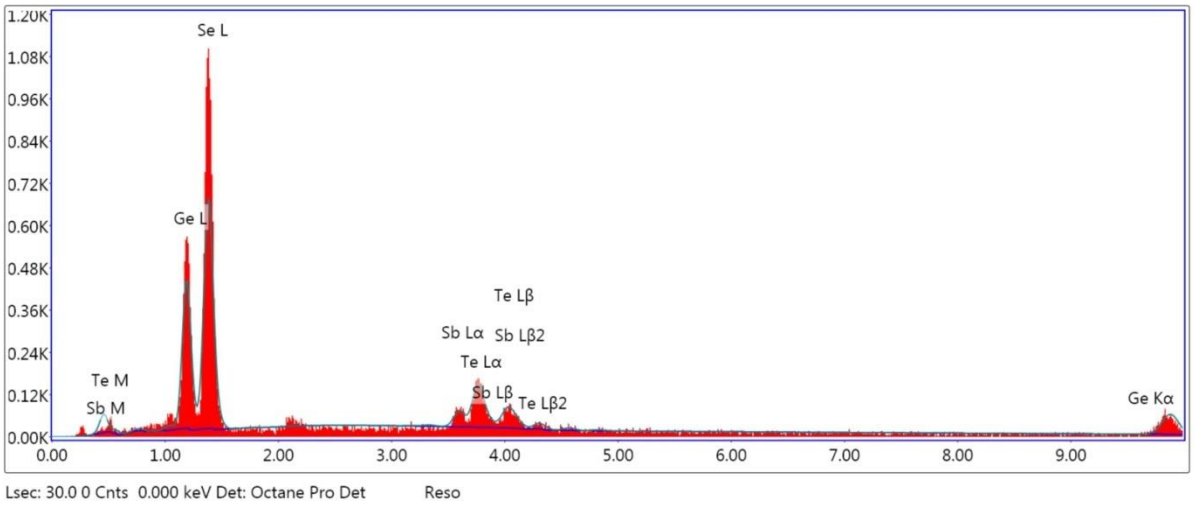

Fig. 1b

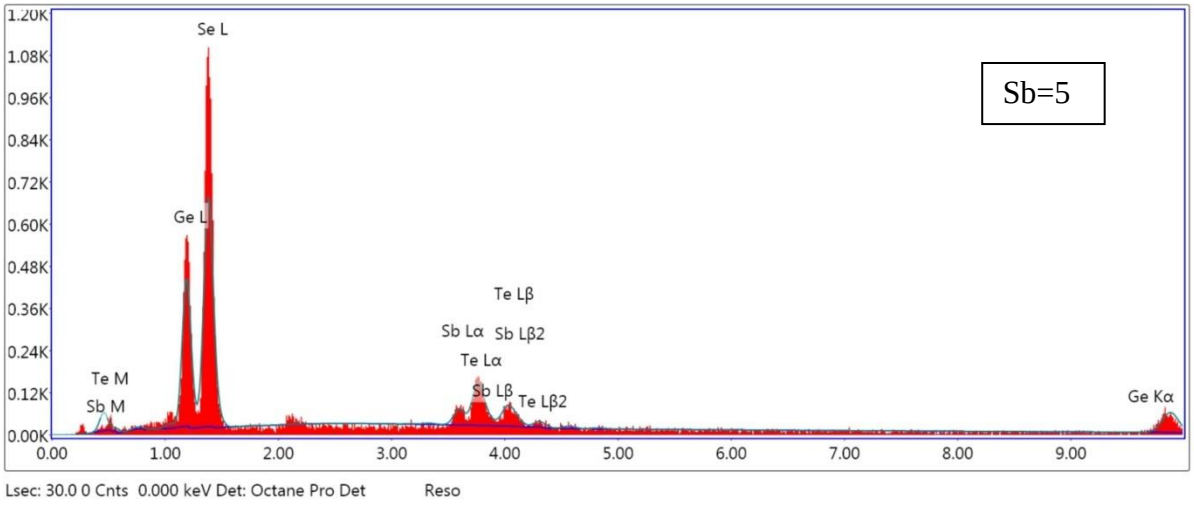

Fig .1c

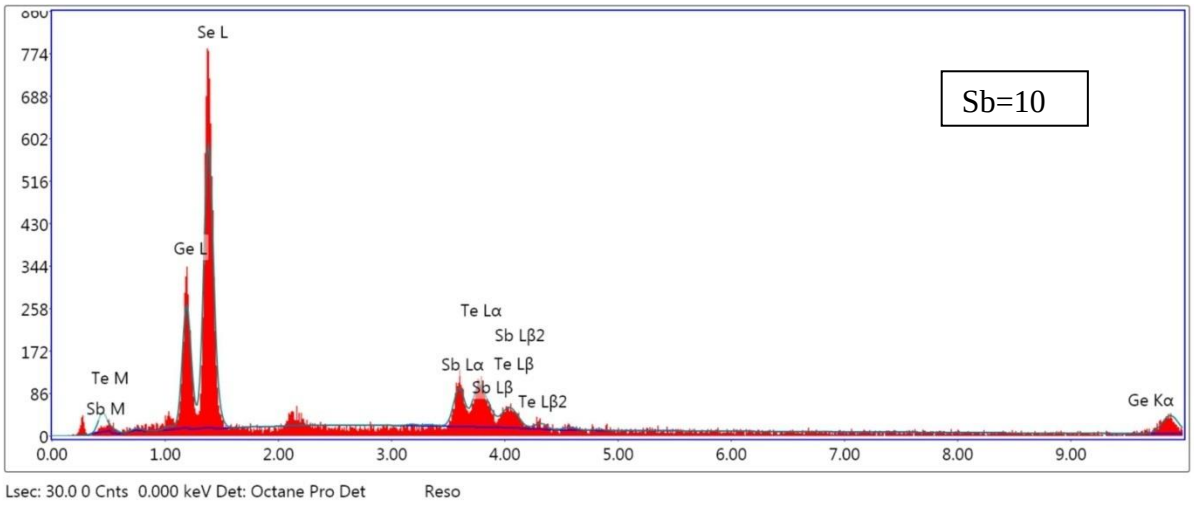

Fig .1d

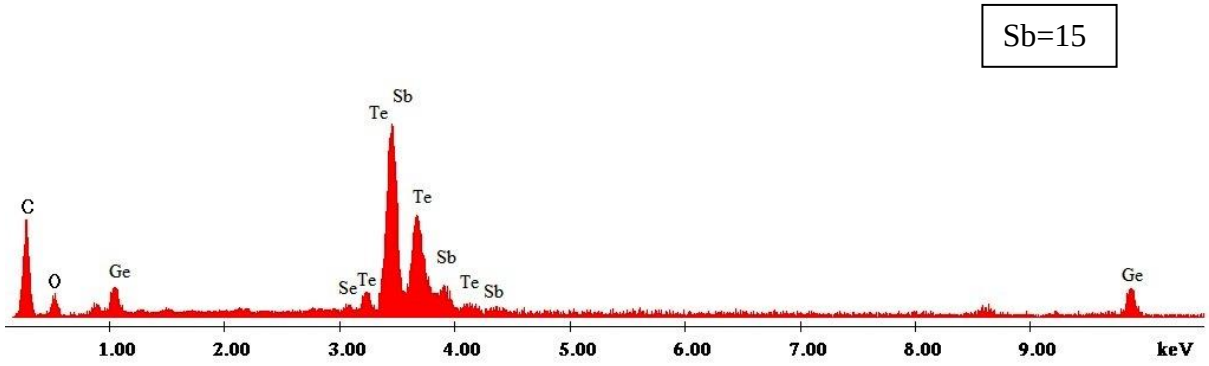

Fig .1e

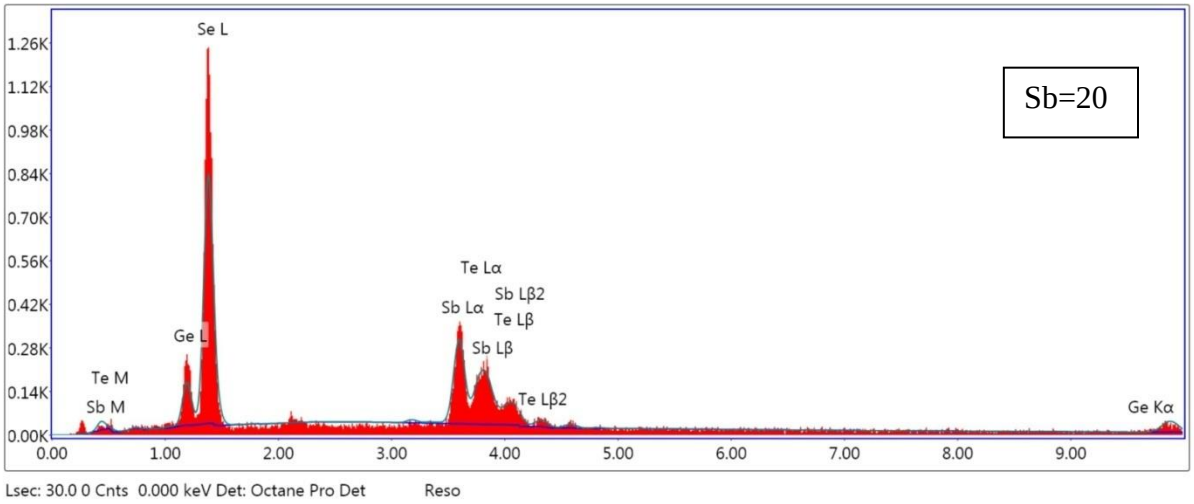

Fig 1(a-e): EDXS for (Ge $_{30-x}$ Sb_xTe_{10} Se $_{60}$) glassy alloys where Sb percentage (0, 5, 10, 15, 20)

Table 1: EDXS results at% and *Sb* percentage of the prepared samples (Ge $_{30-x}$ Sb_xTe_{10} Se $_{60}$) glassy alloys where Sb percentage (0, 5, 10, 15, 20)

No	**Nominal composition at%**				**EDXS results at%**			
	Sb	**Ge**	**Te**	**Se**	**Sb**	**Ge**	**Te**	**Se**
1	0	30	10	60	0.31	26	12	61
2	5	25	10	60	5.26	20.09	13.69	60.96
3	10	20	10	60	9.98	16.27	11.64	62.1
5	20	10	10	60	19.93	8.3	8.72	63.04

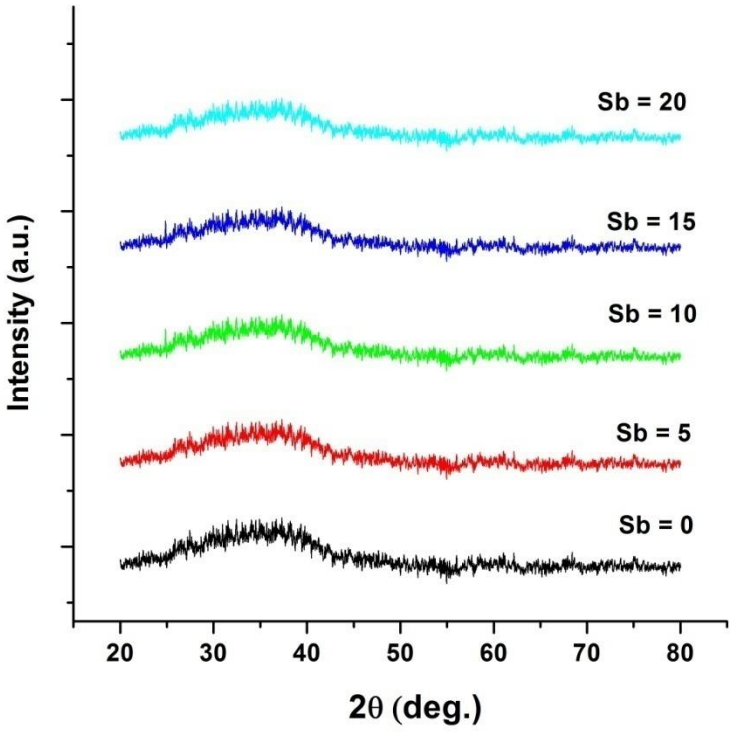

Fig 2: The X-ray diffraction (XRD) pattern for ($Ge_{30-x}Sb_xTe_{10}Se_{60}$) glassy alloys where Sb percentage (0, 5, 10, 15, 20).

Fig 3a

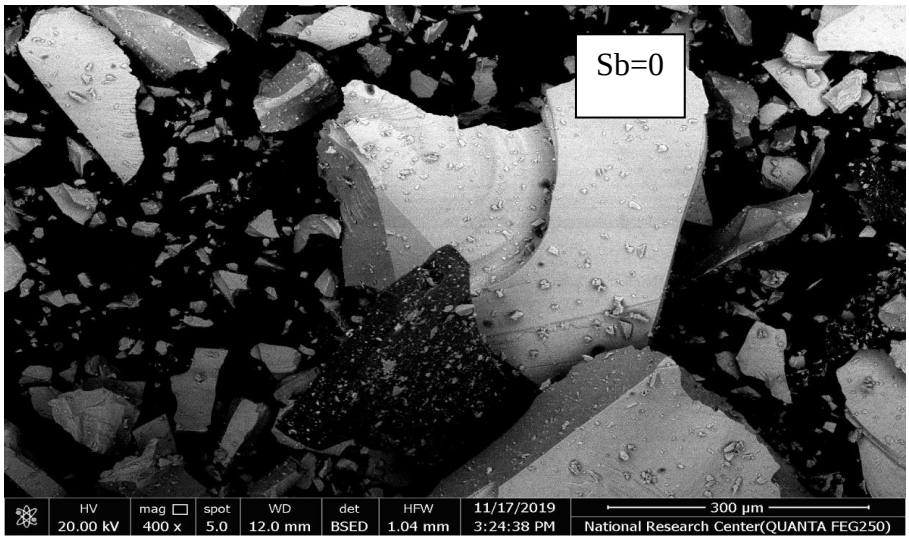

Fig. 3b

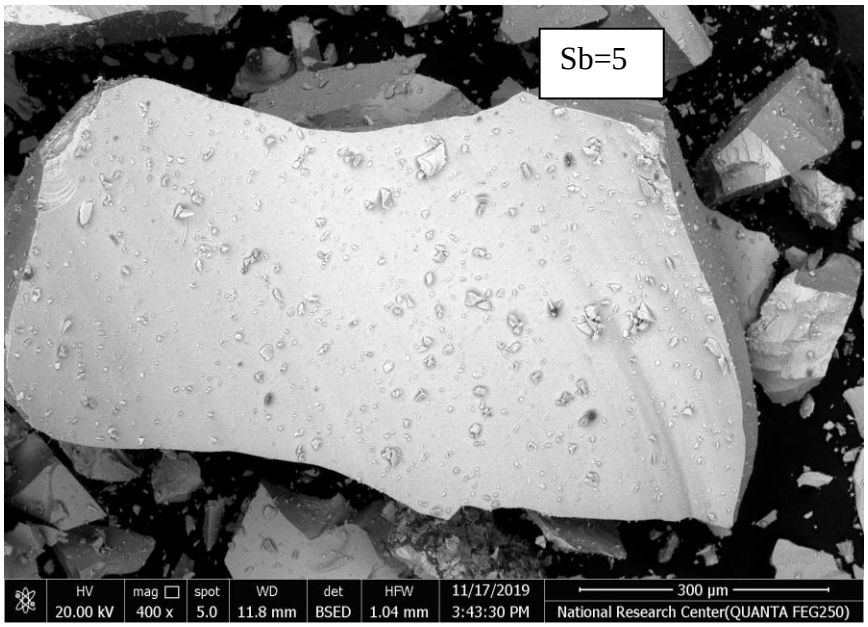
Sb=5
HV
20.00 kV
mag
400 x
spot
5.0
WD
11.8 mm
det
BSED
HFW
1.04 mm
11/17/2019
3:43:30 PM
300 µm
National Research Center(QUANTA FEG250)

Fig. 3c

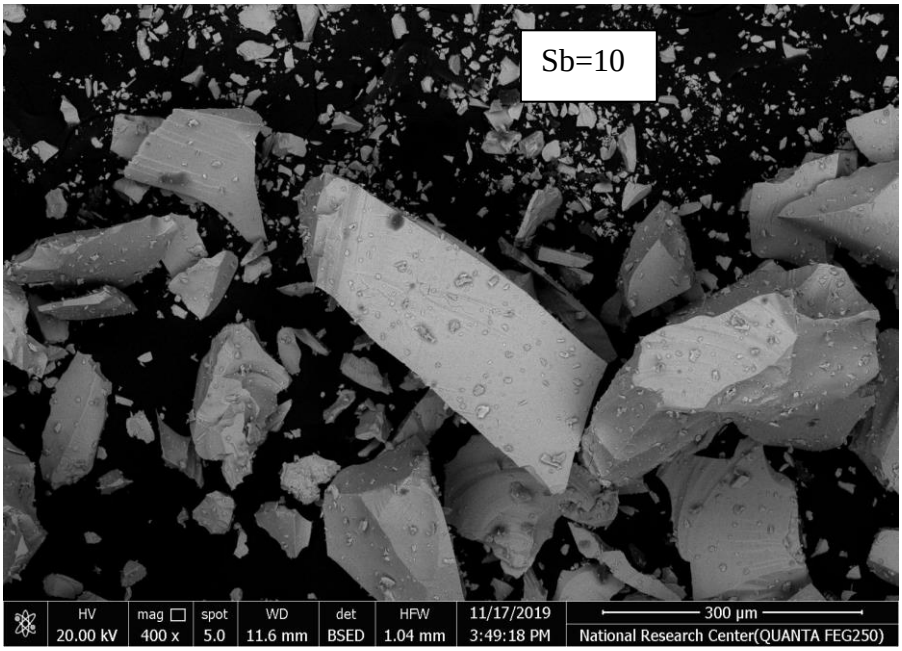
Sb=10
HV
20.00 kV
mag
400 x
spot
5.0
WD
11.6 mm
det
BSED
HFW
1.04 mm
11/17/2019
3:49:18 PM
300 µm
National Research Center(QUANTA FEG250)

Fig. 3d

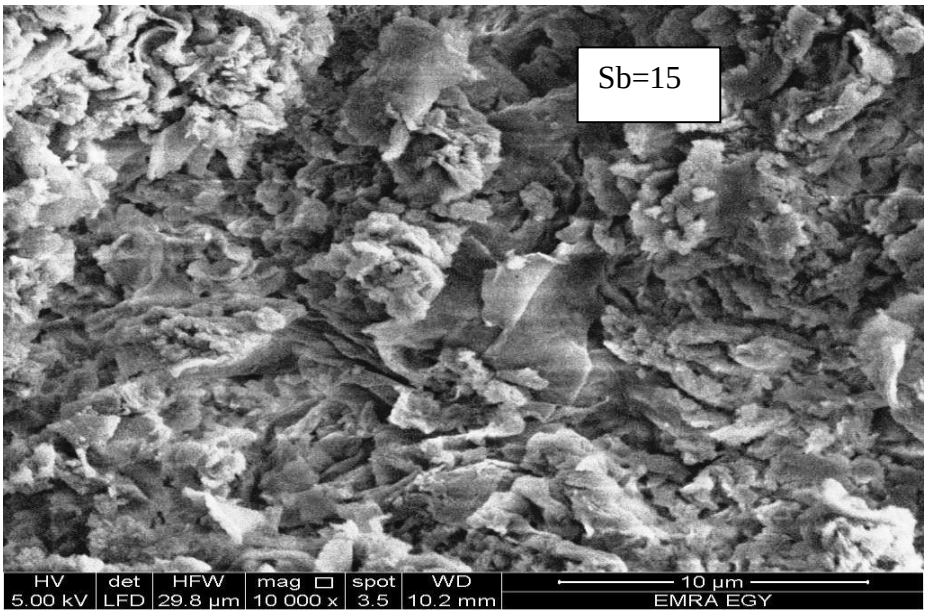

Fig. 3e

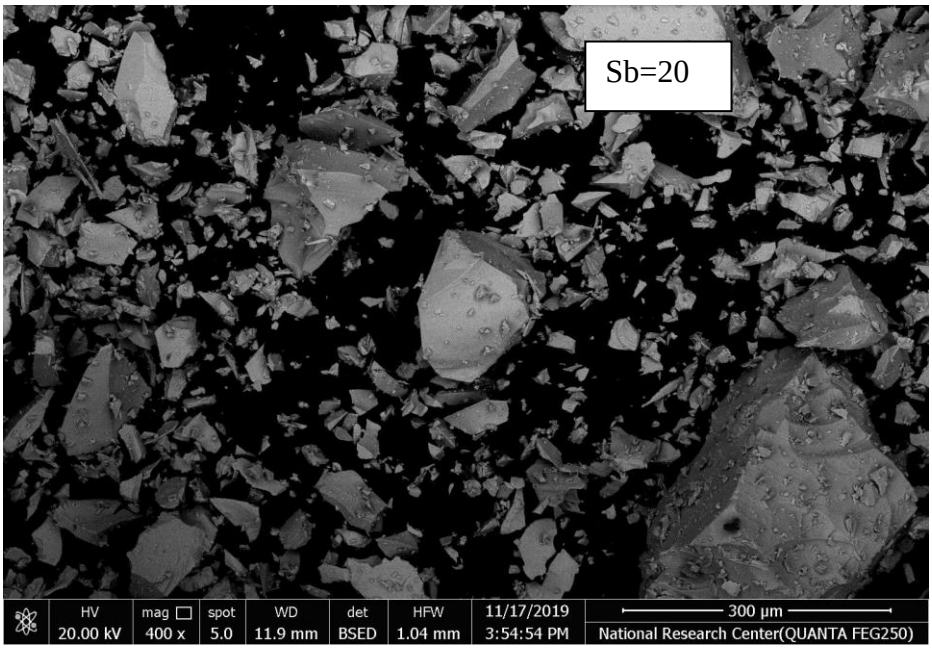

Fig 3(a-e): SEM for $Ge_{30-x}Sb_xTe_{10}Se_{60}$) where Sb percentage (0, 5, 10, 15, 20).

3.2 Optical characterization

3.2 .1 Determination of film thickness and the refractive index

The thin films' optical properties, indicated by their transmittance and reflectance spectra, were measured as a function of wavelength range (400–2500 nm), The T and R with wavelength are shown in **Fig.4**.The homogeneity of the deposited films is demonstrated by the interference fringes in T- spectra at wavelengths (800–2000 nm) that are "non-shrinking" (fringes of equal chromatic order, FECO). Additionally, when the Sb ratio of the Ge-Se-Te glass rises, the absorption edge shifts towards lower photon energies; this is thought to be the consequence of E_g decreasing as Sb replaces Se atoms in the Ge-Se-Te.

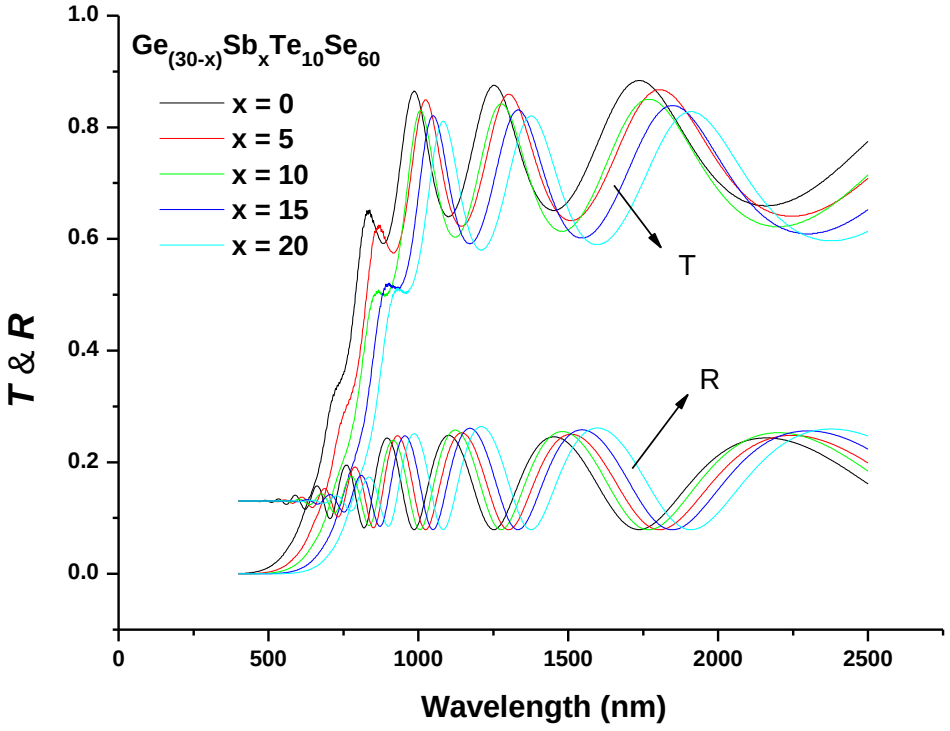

Fig4: Variation of (T) and (R) with wavelength (λ) for $Ge_{30-x}Sb_xTe_{10}Se_{60}$ where (x =0, 5, 10, 15, 20) thin films.

According to the expression derived from (Manifacier et al., 1976),concept for the top and lower interference fringe envelopes in **Fig.5** Swanepoel (Swanepoel,1983)have developed a technique for calculating an approximation of the film n_1 's refractive index in the spectral region of medium and weak absorption according to the equation

$$. n_1 = \left[N + (N^2 - s^2)^{\frac{1}{2}}\right]^{\frac{1}{2}} (1)$$

where

$$N = 2s\frac{T_M - T_m}{T_M T_m} + \frac{s^2 + 1}{2}$$

The maximal and corresponding minimum transmission at this wavelength are denoted by T_M and T_m, respectively. Alternately, one of these numbers represents an extreme of experimental interference, while the other is obtained from the matching envelope; both envelopes were produced using a computer program, the Origin version 8.5 program, utilizing many procedures. On the other hand, the requisite values of the refractive index of the substrate S are calculated by the transmission spectrum of the substrate, T_s using the following equation **(Jenkins & White,1957)**

$$s = \frac{1}{T_s} + (\frac{1}{T_s} - 1)^{\frac{1}{2}} \qquad (2)$$

The fundamental equation for interference fringes must be considered: -

$$2nd = m\lambda \qquad (3)$$

where m is an integer for maximum values and a half-integer for minimum values. Additionally, the film thickness is provided by the following formula if n_{el} and n_{e2} are the refractive indices at two nearby maxima (or minima) at λ_1 and λ_2, respectively.

$$d = \frac{\lambda_1 \lambda_2}{2(\lambda_1 n_{e2} - \lambda_2 n_{e1})} \qquad (4)$$

For all the films being studied, the results for *d* given by this equation are roughly 1000 nm.

Fig.5a

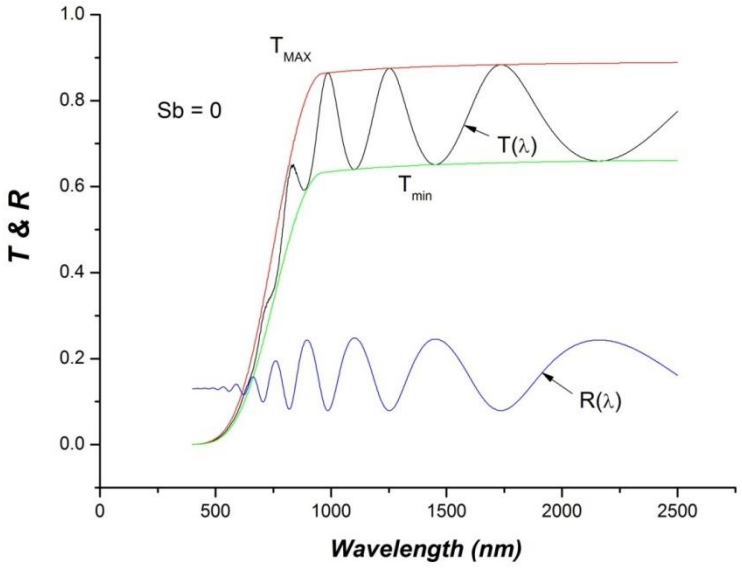

Fig. 5b

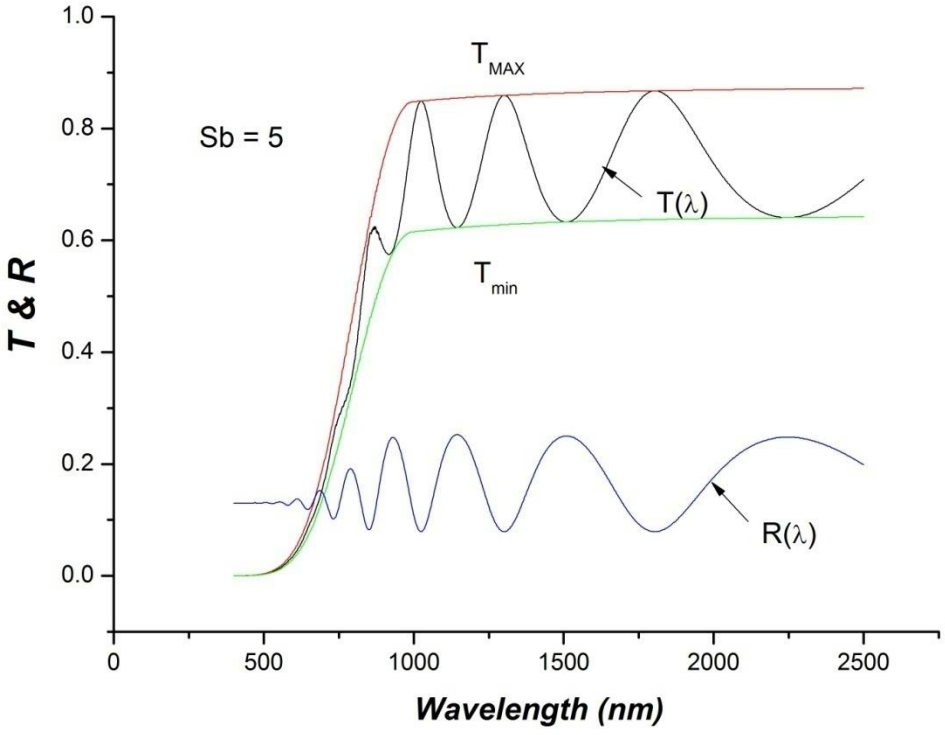

Fig. 5c

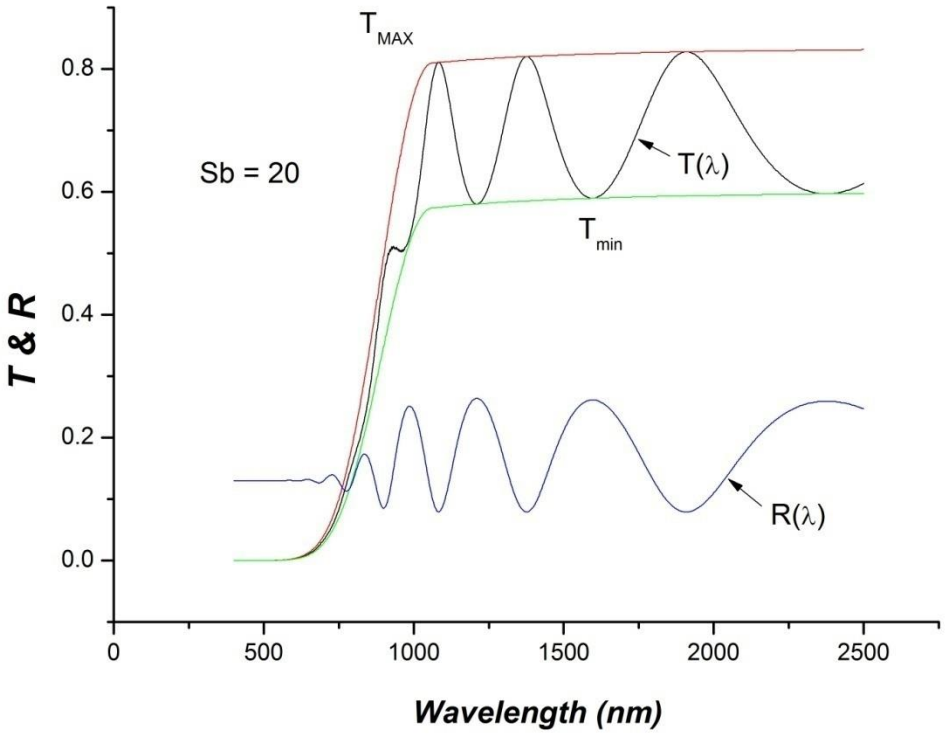

Fig. 5(a-c). Transmittance (T) and Reflectance(R) spectra of (a) Ge_{30} Sb_0Te_{10} Se_{60}, (b) $Ge_{25}Sb_5Te_{10}$ Se_{60}(c) $Ge_{10}Sb_{10}Te_{10}Se_{60}$. The top and bottom transmittance envelope T_{max} and T_{min}shown as red line and green line, respectively

.

The two-term Cauchy function, $n(\lambda) = B + A/\lambda_2$ can be utilized as an appropriate dispersion function for estimating values of *n* where that function can be used for extrapolation the whole wavelength dependence of refractive index .The values of Cauchy coefficient, A and B are presented in **Table 2**. **Fig.6** illustrate n values vs. λ, for different compositions, the figure indicates that over the whole spectral range under investigation, *n* values rises with increasing Sb concentration. This increase can be described in terms of polarizability, where Sb has greater polarizability than Se due to its higher atomic radius of 1.53 A◦ compared to Se atoms' atomic radius of 1.22 A˚.

Table2: The fitted Cauchy coefficient, optical band gap E_g, the single-oscillator energy E_0,dispersion energy E_d, refractive index *n(o)* at $(E \rightarrow 0)$, and non-linear refractive index forn_2 Ge_{30-x} Sb_xTe_{10} Se_{60} where (x =0, 5, 10, 15, 20) glassy compositions as a function of Sb% content

Sb%	Cauchy Coefficient		$E_g(eV)$	$E_e(eV)$	$E_d(eV)$	$E_o(eV)$	n_o	$n_2 x10^{-10}$(esu)
	A	B						
0	8.9	2.6	1.375	0.29	26.47	3.89	2.796	1.99
5	10.4	2.6	1.311	0.34	25.51	3.60	2.854	2.35
10	12.4	2.7	1.200	0.36	24.35	3.31	2.911	2.76
15	15.7	2.6	1.193	0.38	22.55	2.98	2.969	3.23
20	21.0	2.5	1.009	0.40	20.19	2.62	3.022	3.730

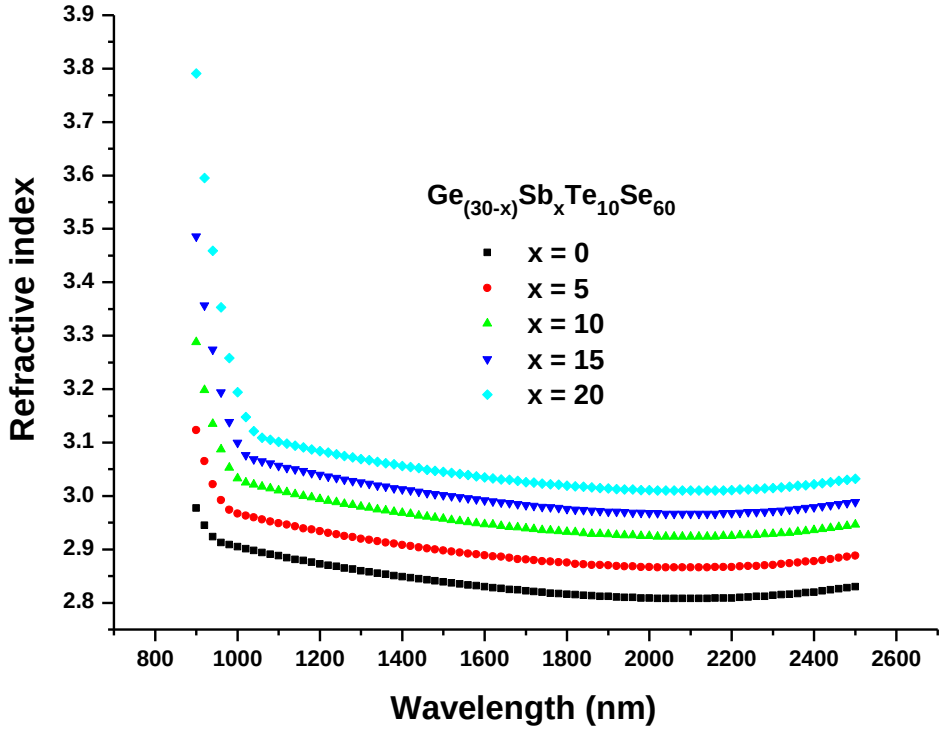

Fig. 6 : *n* vs. λ, for $Ge_{30-x}Sb_xTe_{10}Se_{60}$ where (x =0, 5, 10, 15, 20)

The dispersion relationship of Wemple and DiDomenico (MDD model)(Wemple and DiDomenico,1971) can be utilized for fitting the energy reliance of *n* in amorphous materials. Here, E_0 is the single-oscillator energy and E_d is the dispersion energy.

$$n^2 - 1 = \frac{E_o E_d}{E_o^2 - (h\nu)^2} \qquad (5)$$

Fig.7 illustrates how to expand the data to a straight line and plot $(n^2 - 1)^{-1}$ versus $(h\nu)^2$ to derive E_0 and E_d from the intercept, E_0/E_d, and the slope, $-1/E_0E_d$. the values of the refractive index $n(0)$ at $h\nu = 0$ for the prepared films are illustrated in **Fig.7**,the values of $n(0)$ are shown in **Table 2** and the presented values indicate that $n(0)$ increase with declining of Sb content.

The derived values of E_d and E_0 for the thin film samples are listed in **Table 2**, and the values presented indicate that E_o, alters roughly in relation to E_g ($E_o \approx 2E_g$) (Tanaka,1980), E_d declined with increasing Sb concentration, this decline can be described in term of the bonds where the Se-Se homopolar bonds decline with increasing Sb content according to calculations made in the author's earlier work **(Soraya *et al.*, 2020).**This indicates that Sb is more coordinated in the

glass matrix. E_d or E_o, considered as a gauge for the strength of transitions between interband **(Krbal *et al*., 1971).**

A notable accomplishment of WDD model is the empirical relationship that related E_d, to other physical parameters of the material through the coming equation **(Wemple & DiDomenico,1971) :**

$$E_d = \beta N_c Z_a N_e \,(ev) \qquad (6)$$

$E_d = \beta N_c Z_a N_e (eV)$where N_c defined as the closest cation's effective coordination number to the anion.

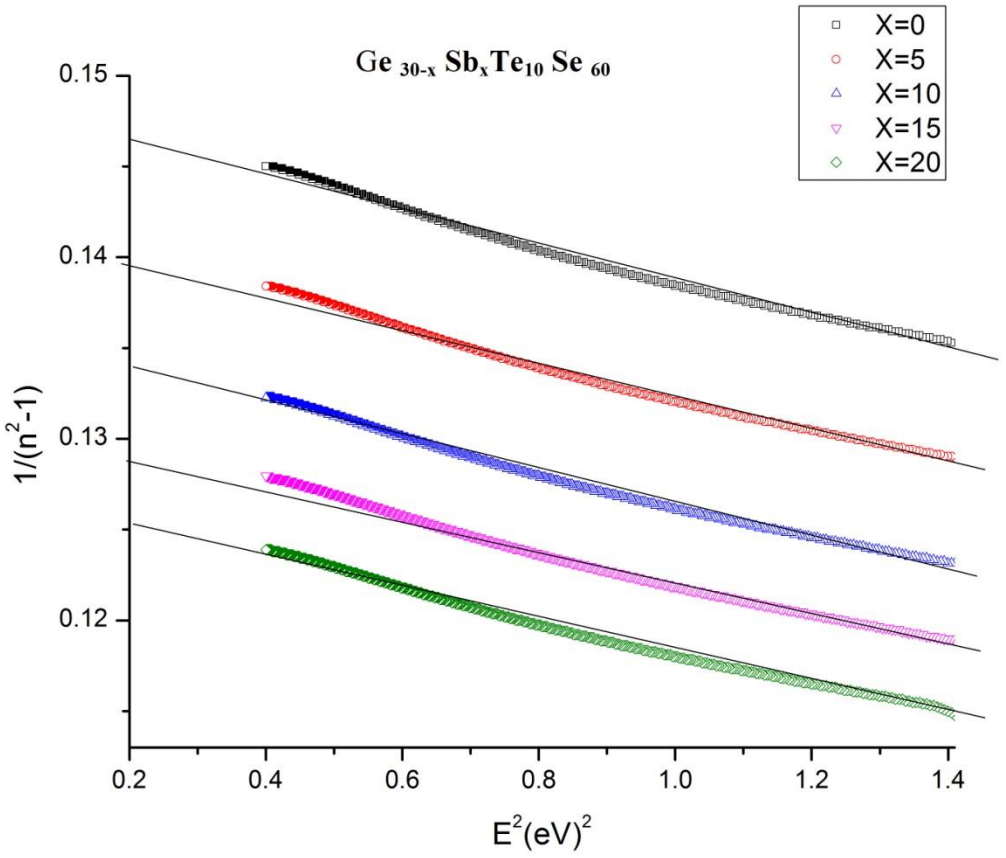

Fig.7: $(n^2\text{-}1)^{-1}$ vsE^2 for Ge $_{30\text{-}x}$ Sb_xTe_{10} Se $_{60}$ where (x =0, 5, 10, 15, 20)

The effective coordination number of the cation nearest neighbor to the anion, Z_a is the anion's formal chemical valence, N_e is the effective number of valence electrons in an anion, and for

covalent crystalline and amorphous materials β = 0.37±0.04 eV. The decrease in N_c causes the decline of E_d with increasing Sb concentration.

3.2.2 Computing the absorption coefficient, the extinction coefficient, and optical band gap

The experimentally values of R and T which measured by the two-beam spectrophotometer can be used to derive the absorption coefficient α in the strong absorption range according to the following equation **(Vahalova *et al*., 2000)**:

$$\alpha = \frac{1}{d} \ln \left[\frac{(1-R)^2 + \left[(1-R)^4 + 4R^2T^2 \right]^{1/2}}{2T} \right] \qquad (7)$$

where d is the film thickness. **Fig.8** shows α according to photon energy for the various compositions of $Ge_{30-x}\ Sb_xTe_{10}\ Se_{60}$ where (x =0, 5, 10, 15, 20).It is demonstrated that the basic absorption edge ($\alpha \geq 10^4$), in all the thin films under study, changes towards the lower photon energy with increasing Sb concentrations. Certainly, that is having a strong relation to the decline of E_g with the insertion of Sb in these compositions.

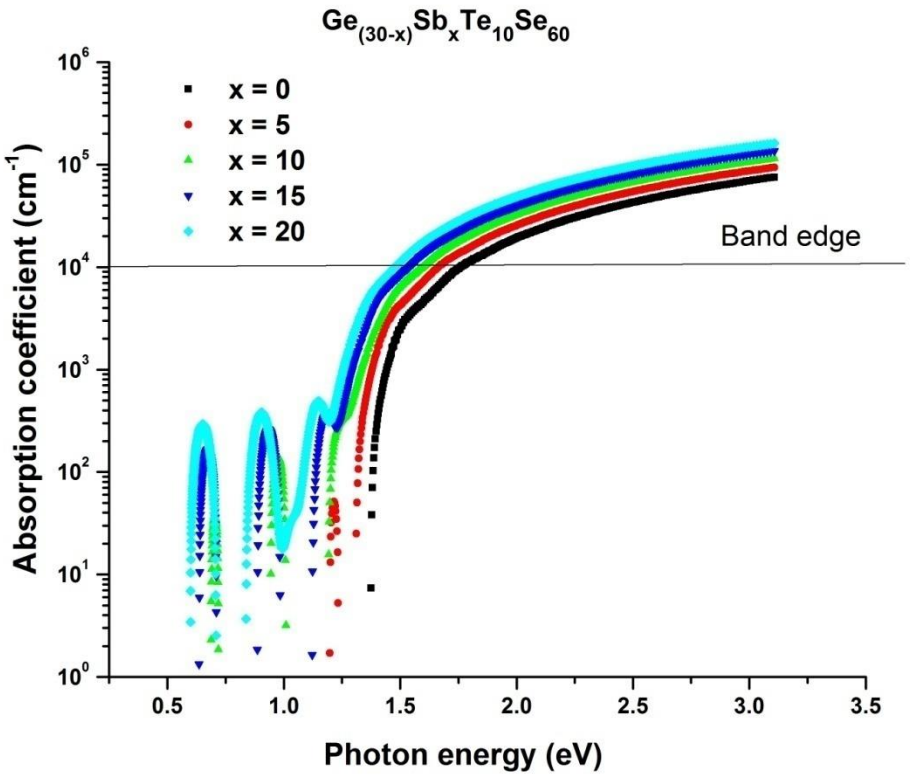

Fig.8: The absorption coefficient vs photon energy Ge $_{30-x}$ Sb$_x$Te$_{10}$ Se $_{60}$ where (x =0, 5, 10, 15, 20).

The values of λ and α are using to compute the extinction coefficient k from the formula $k = \frac{\alpha\lambda}{4\pi} k = \alpha\lambda/4\pi$. **Fig.9** plots the values of k vs λ, for different compositions Ge 30-x SbxTe10 Se 60, the graph indicates the dependence of k on λ.

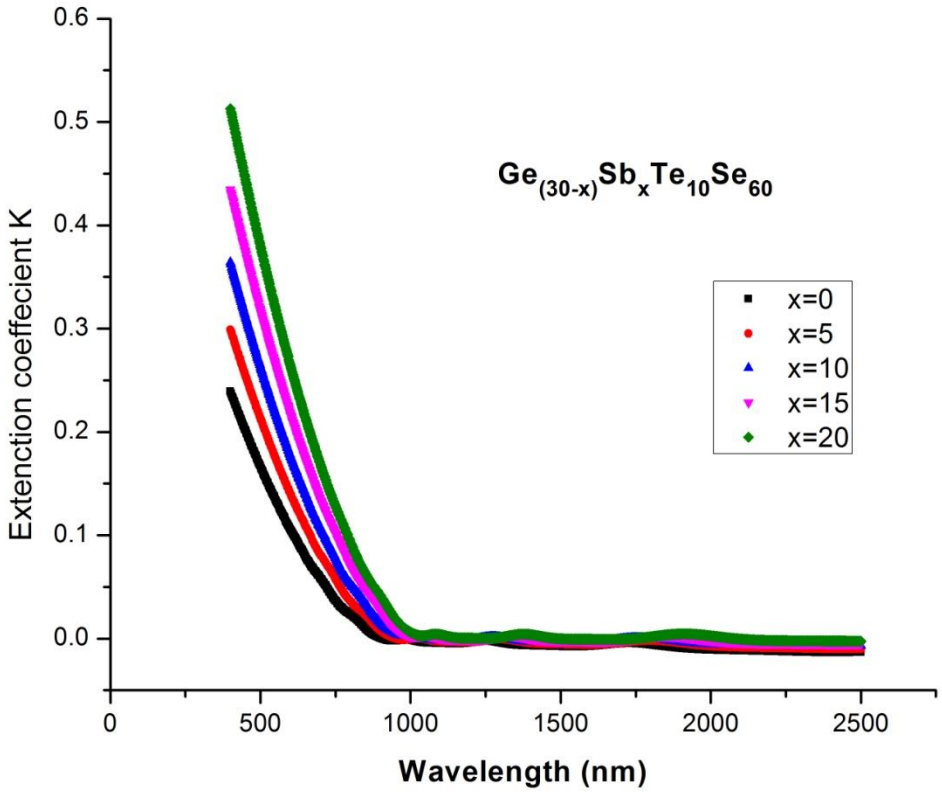

Fig.9: the extinction coefficient *k* vs. λ, for Ge $_{30-x}$ Sb_xTe_{10} Se $_{60}$ where (x =0, 5, 10, 15, 20)

Tauc's relation **(Tauc,2012)** is used to calculate α in the high-absorption region ($\alpha \geq 10^4$) by the following expression: -

$$(\propto h\nu)^{\frac{1}{2}} = C(h\nu - E_g^{opt}) \qquad (8)$$

Where *C* is a constant that related to the probability of the transition, and the optical band gapE_g^{opt}. For the various compositions of the thin films under investigation.

Fig.10 demonstrates a good matching of $(\alpha h\nu)^{1/2}$ versus $(h\nu)$. The intercept of $(\alpha h\nu)^{1/2}$ vs non-direct transition was used to get the values of E_g^{opt}. The calculated values of E_g for each film presented in **Table.2** and showed a drop in the value of E_g from 1.375 to 1.009 eV, E_g of the films decline with increasing Sb concentration.

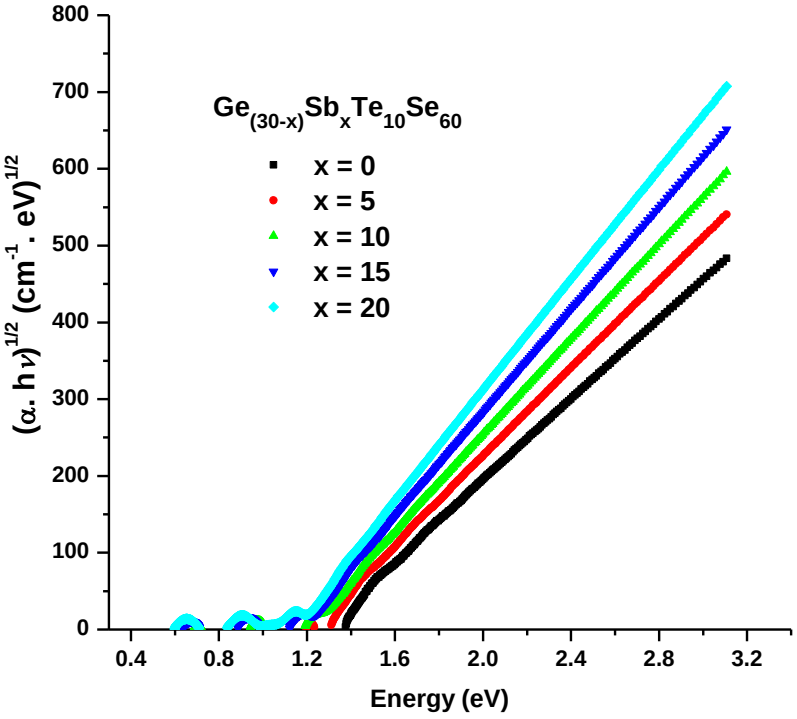

Fig.10: $(\alpha h\nu)^{1/2}$vs photon energy, for Ge $_{30-x}$ Sb_xTe_{10} Se $_{60}$ where (x =0, 5, 10, 15, 20) to estimate the values of (E_g^{opt}).

At smaller values of α where ($1 \leq \alpha \leq 10^4 cm^{-1}$), Urbach relation(Urbach,1953) describes the exponential depends of the absorption on the photon energy by the equation:

$$\alpha(h\upsilon) = \alpha_0 \exp\left(\frac{h\upsilon}{E_e}\right) \qquad (9)$$

where α_0 is a constant and E_e is the Urbach energy which is pertaining to the width of the localized states' band tail at the conduction or valence band edge.

Fig.11, which depicts *ln(α)* vis *E*, indicates the dependence of the ln(α) on *E*for the various samples. **Fig.11** has been used to estimate E_e by expanding the data to a straight line and plot*ln(α)* vs *E* to derive E_e from the slope. The estimated values of E_e are shown in **Table 2** and indicate that E_g^{opt} decreases with increasing Sb content ,while E_e shows the reverse tendency, where E_e values increase from 0.29 eV to 0.4 eV whereas E_g^{opt} values fall from

1.375 to 1.009 eV as the Sb content is raised from 0 to 20 at. % in the thin films under investigation.

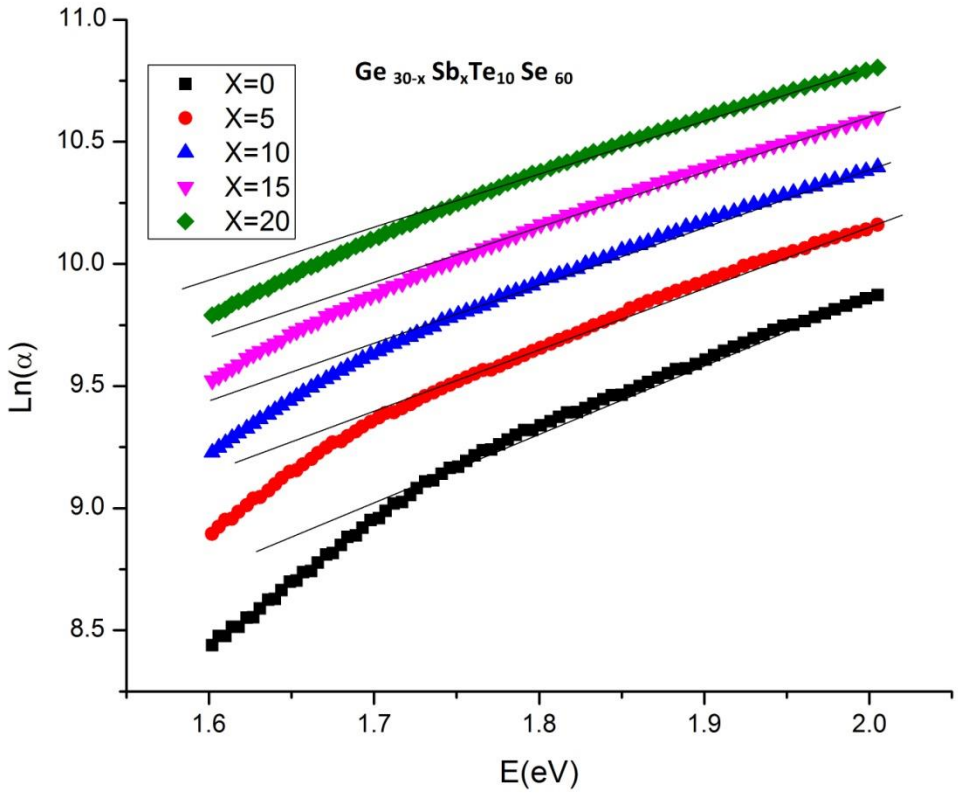

Fig.11: *ln(α)*vs(*hν*) for Ge $_{30-x}$ Sb$_x$Te$_{10}$ Se $_{60}$amorphous films, to estimate the Urbach energy E$_g$.

The propensity of E$_g$ to decline with rising Sb concentrations in the current work can be described in view of the following points;

1. the average single bond energy is a useful factor in understanding the variance of E$_g$, where that factor describes the bond strength , this factor is calculated from the ratio of the average heat of atomization H_s and the average coordination numbers N_c , this ratio (H_s/N_c) was computed in the author's earlier work **(Soraya *et al.*, 2023)** , the bond strength (H_s/N_c) shows a reduction with a rise in Sb content; correspondingly leading to a reduction in E_g .
2. As indicated by Davis and Mott's article **(Davis & Mott, N, 1970)** that the lower values of optical gap are caused by the high density of localized states in the band structure; density of localized states can be described regarded to Urbach energy E$_e$ which is pertaining to the width of the localized states' band tail at the band edge of conduction or valence, the values of E$_e$ is

presented in **Table1** and that values indicate that the E_e rises as the Sb concentration rises ,whereas E_g^{opt} decreases, this implies that the localized states inside the band gap increase with increasing Sb contents in the current samples

3. Kastner **(Kastner *et al.*, 1976)** reported that chalcogenide's valence band is composed of lone pair p-orbitals that are provided by the chalcogen atoms, these lone pair electrons will have higher energy than those of electronegative atoms and adjacent to electropositive atoms. Hence, the addition of electropositive elements to the system will enhance the energy of the lone pair and the valence band moves toward the energy gap, subsequently the decline of E_g with rising Sb concentrations in the current work.

3.2 .3 Computing the dielectric constants and loss factor.

The electrical applications directly depend on the dielectric characteristics; therefore, it is crucial to ascertain the dielectric constants of these compositions under research. The real and imaginary components of the dielectric constant, ε_r and ε_i, respectively, are *n* and the extinction coefficient *K* and may be computed using the formulas listed below **(Shaaban *et al*.,2014):**

$$\varepsilon_r = n^2 - K^2 \qquad (10)$$

$$\varepsilon_i = 2nk \qquad (11)$$

For the films under examination, **Fig.12,13** present the relation of ε_r and ε_i with wavelength, the figures indicate that ε_r and ε_i constants are decreasing as wavelength of the incident photon increases. As shown in **Fig.12,13**, the imaginary part ε_i reaches its minimal value first then the real part ε_r which gradually falls after that. These outcomes confirm that ε_i refers to how much of an electric field can a dielectric substance absorb due to dipole motion, while ε_r explains how far the substance slows down the speed of electromagnetic waves **(Bakr *et al*.,2011)**.

The estimated values of ε_r and ε_i can be used to determine the $tan\ tan\ \delta$ which is ratio of ε_i and ε_r **(Shaaban *et al*.,2013)**:

$$tan\ tan\ \delta = \frac{\varepsilon_i}{\varepsilon_r} \qquad (12)$$

Fig.14 presented the variance of $tan\ tan\ \delta$ vs (hv), and the figure indicates that$tan\ tan\ \delta$ raiseswith (hv) increases

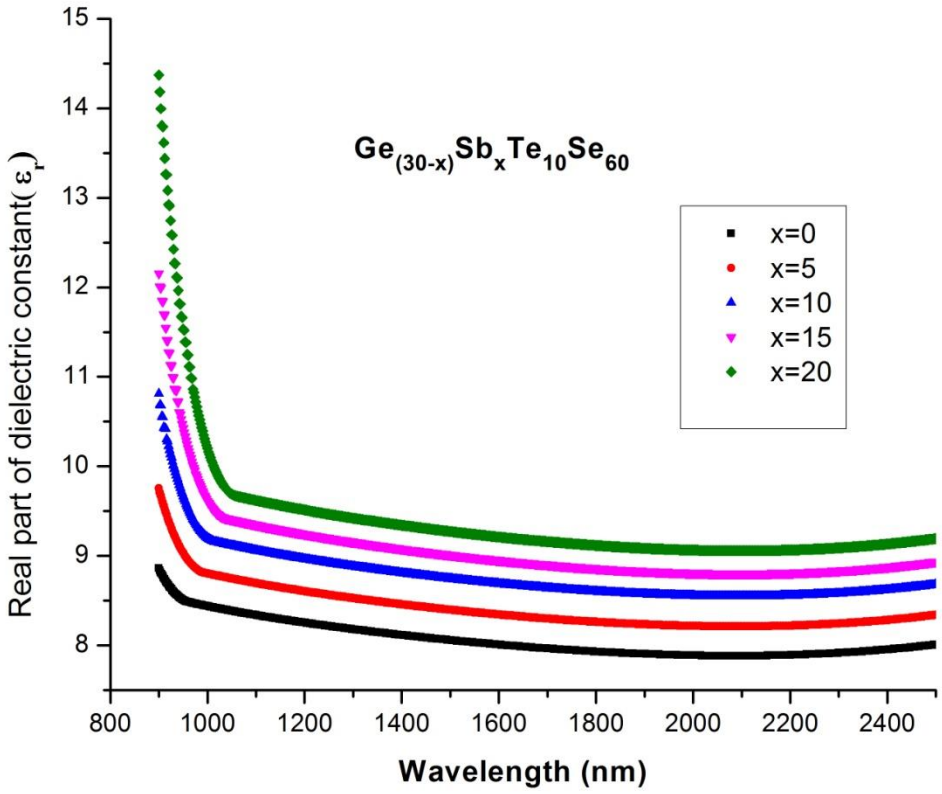

Fig.12 : ε_r vs λ for Ge_{30-x} Sb_xTe_{10} Se_{60} where (x =0, 5, 10, 15, 20) thin films

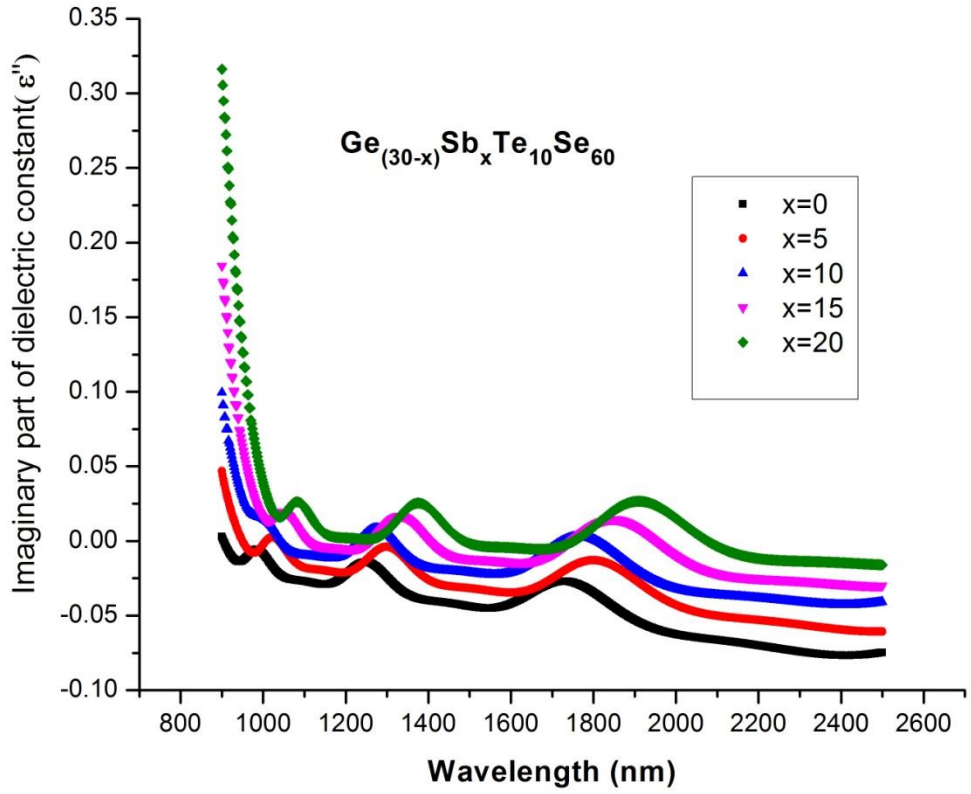

Fig.13: $\varepsilon_i$vsλ for Ge $_{30-x}$ $Sb_xTe_{10}Se_{60}$ where (x =0, 5, 10, 15, 20) thin films

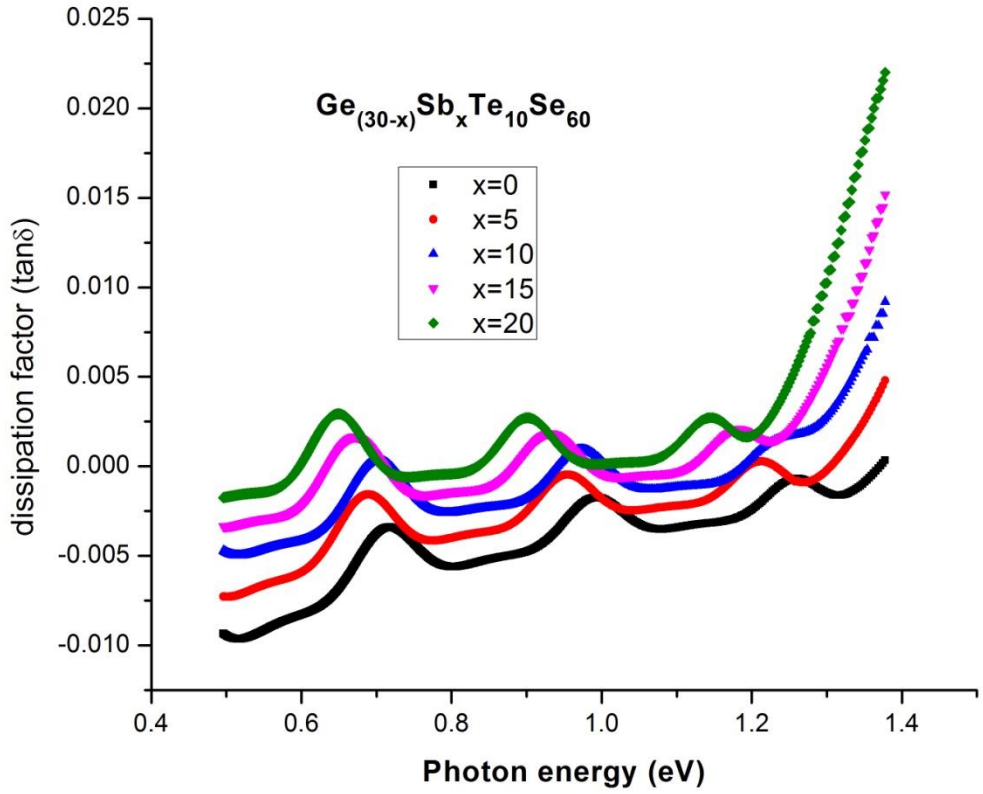

Fig.14:tan (δ)vs photon energy for Ge $_{30-x}$ Sb_xTe_{10} Se $_{60}$ where (x =0, 5, 10, 15, 20) thin films

3.2.4 Computing of non-linear refractive index

The non-linear effects take place when intense light is transmitted across the material, the incident intensity has a significant impact on the non-linear refractive indexn_2 of chalcogenide glasses. When The material is exposed to a powerful electric field. from incident light; The polarization refers to the extension of polarizability by a factor that is proportional to the square of the electric field, and no longer proportional to electric field **(Sharma & Katyal,2010)**

According to Tichy and Ticha relationship **(Ticha & Tichy, 2002)**, the nonlinear refractive index n_2 was determined. The third order non-linear susceptibility $S^{(3)}$ should be determined first , which is obtained using the following relation **(Wang, 1970)**

$$S^{(3)} = A\left[S^{(1)}\right]^4 \qquad (13)$$

$$S^{(3)} = \frac{A}{(4\pi)^4}(n_o^2 - 1)^4 \qquad (14)$$

where A = 1.7 x10^{-10} (for $S^{(3)}$ in esu)

Miller's rule, which has gained popularity, and the static refractive index calculated from the WDD model combine to form the Tichy and Ticha connection **(Ticha &Tichy, 2002; Shaaban *et al*.,2019).**

$$n_2 = \left[\frac{12\pi}{n_o}\right] S^{(3)} \qquad (15)$$

n_2 derived for each film is presented in **Table 2**, It is evident that n_2 index increases with increasing antimony concentration in samples.

The crucial factors for obtaining high susceptibility are band gap and polarizability, **Fig.15** presents ($S^{(3)}$) and E_g variation with Sb content, and the figure indicates that when Sb is added to **GeSeTe** composition, $S^{(3)}$ increases while E_g decreases

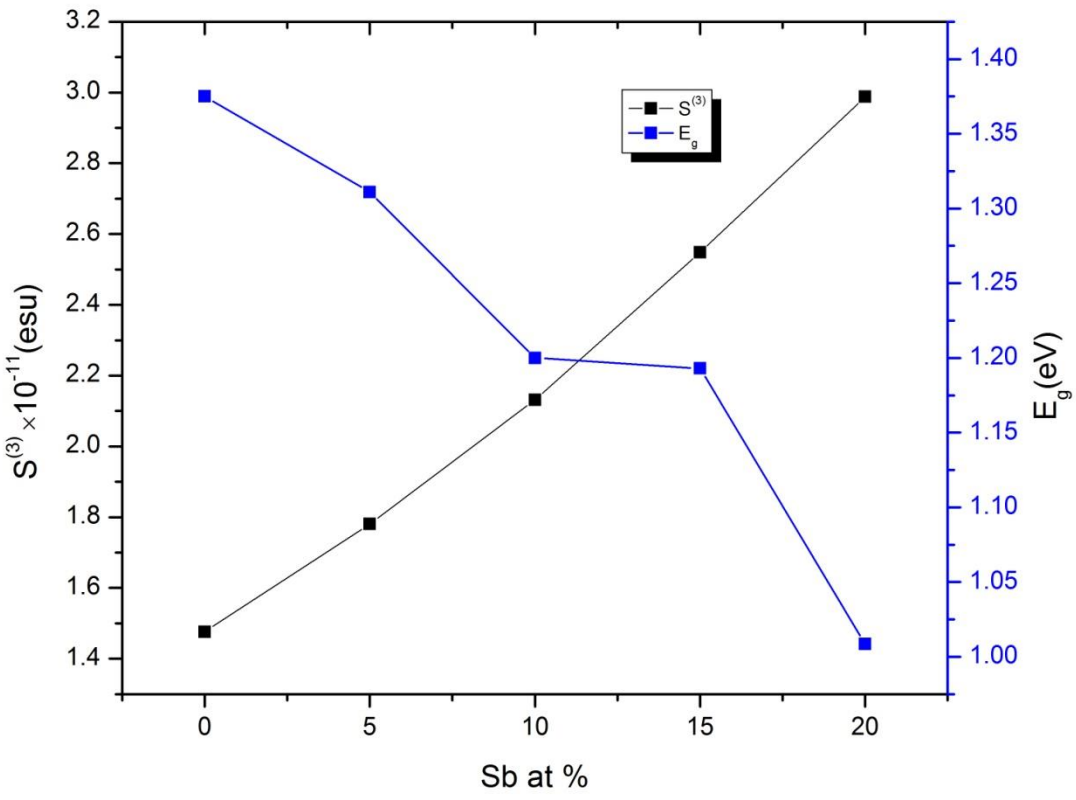

Fig.15: ($S^{(3)}$) and $E_g$vs Sb content for for $Ge_{30-x}Sb_xTe_{10}Se_{60}$ where (x =0, 5, 10, 15, 20) thin films

The basis of Tauc gap and defect states **(Gopinath *et al*.,2004; Petit *et al*.,2009)**can be used to explain non-linearity of glasses, nonlinearity is determined from Tauc gap values according to Moss rule **(Moss, 1985)** ,the presence of heteropolar and homopolar bonds is the reason of decreasing E_g^{opt} and increasing n_2 with the increasing Sb content **(Gopinath *et al*.,2004; Petit *et al*.,2009)**. Far-infrared studies has confirmed that increase in n_2 is due to the presence of $GeSe_4$ (ν2 mode), Se_6Te_2 rings, $GeTe_4$ tetrahedron, and Te-Te structural units **(Sharma *et al*., 2013).**

4.Conclusion

The work studies the optical characterization of $Ge_{30-x}Sb_xTe_{10}Se_{60}$thin films. The refractive *n* rises as Sb concentration increase over the whole spectral range under investigation, this increase can be described in terms of polarizability, where Sb has greater polarizability than Se due to its higher atomic radius of 1.53 A◦ compared to Se atoms' atomic radius of 1.22 A◦.E_g values of the examined films were observed to decline with raising Antimony content where the value of E_g declined from 1.375 to 1.0091 eV. The propensity of E_g to decline with rising Sb concentrations has been described in view of the average single bond energy, Urbach energy as an indicator to density of localized states in the band structure, and the difference in the relevant elements' electronegativity. The dispersion relationship of Wemple and DiDomenico was utilized to drive the single-oscillator energy E_0, the dispersion energy E_d , and $n(0)$ .The obtained results show that $n(0)$ increase with declining of Sb content ,E_o, alters roughly in proportion to the optical band gap ($E_o \approx 2E_g$) , and E_d decline with increasing Sb concentration, this decline can be described in term of the bonds where the Se-Se homopolar bonds decline with increasing Sb content. The values of the real and imaginary of the dielectric constant was estimated and be used to determine the loss factor (dissipation factor)$tan\ tan\ \delta$ the estimated values show that $tan\ tan\ \delta$ increases as ($h\nu$) increases. Tichy and Ticha relationship was used to determine non liner refractive index n_2, the obtained values indicate that n_2 increases with increasing antimony concentration in samples, Moss rule was used to explain increasing n_2 with the increasing Sb content due to the presence of heteropolar and homopolar bonds is the reason of decreasing.$Ge_{30-x}Sb_xTe_{10}Se_{60}$ compassions are promising materials and may find their full interest for nonlinear optics in the mid-infrared range because of their low optical band gap energies. These materials are appealing in the field of mid-IR sensing and optical nonlinear devices due to their wide IR transparency and high non-linear refractive indices.

References:

Abbady, G., & Abd-Elnaiem, A. M. (2019). Thermal stability and crystallization kinetics of Ge13In8Se79 chalcogenide glass. *Phase Transitions*, *92*(7), 667-682.

Abdel-Wahab, F., Badawi, A., Alatibi, M. S., Alomairy, S. E., Ashraf, I. M., & Ahmed, E. M. (2017). Spectroscopic ellipsometry characterization of Ge30-xSbx Se70 films using combinations of multiple dispersion functions. *Optik*, *147*, 59-71.

Abdel-Wahab, F., El Shaikh, H. A., & Salem, R. M. (2013). Effect of Sb on the optical properties of the Ge–Se chalcogenide thin films. *Physica B: Condensed Matter*, *422*, 40-46.

Abdel-Wahab, F., Karar, N. A., & Merazga, A. (2020). Time dependent bond arrangement approach to photo-induced changes in Ge30-xSbxSe70 thin films. *Materials Chemistry and Physics*, *242*, 122521.

Akl, A. A., & Hassanien, A. S. (2015). Microstructure and crystal imperfections of nanosized CdSxSe1− x thermally evaporated thin films. *Superlattices and Microstructures*, *85*, 67-81.

Bakr, N. A., Funde, A. M., Waman, V. S., Kamble, M. M., Hawaldar, R. R., Amalnerkar, D. P., ... & Jadkar, S. R. (2011). Determination of the optical parameters of a-Si: H thin films deposited by hot wire–chemical vapour deposition technique using transmission spectrum only. *Pramana*, *76*, 519-531.

Bavafa, P., & Rezvani, M. (2018). Effect of Sn doping in optical properties of Se-Ge glass and glass-ceramics. *Results in Physics*, *10*, 777-783.

Behera, J. K., Zhou, X., Tominaga, J., & Simpson, R. E. (2017). Laser switching and characterisation of chalcogenides: systems, measurements, and applicability to photonics. *Optical Materials Express*, *7*(10), 3741-3759.

Beyer, W., Mell, H., & Stuke, J. (1971). Conductivity and thermoelectric power of trigonal SexTe1− x single crystals. *physica status solidi (b)*, *45*(1), 153-162.

Chauhan, R., Srivastava, A. K., Mishra, M., & Srivastava, K. K. (2010). Effect of UV exposure on some optical properties of As-Se based chalcogenide glasses. *Integrated Ferroelectrics*, *119*(1), 22-32.

Chen, B., Chen, G., Wang, W., Cai, H., Yao, L., Chen, S., & Huang, Z. (2018). Magnetron sputtering deposition of GeSe thin films for solar cells. *Solar Energy*, *176*, 98-103.

Davis, E. A., & Mott, N. (1970). Conduction in non-crystalline systems V. Conductivity, optical absorption and photoconductivity in amorphous semiconductors. *Philosophical magazine*, *22*(179), 0903-0922..

Désévédavy, F., Renversez, G., Troles, J., Houizot, P., Brilland, L., Vasilief, I., ... & Adam, J. L. (2010). Chalcogenide glass hollow core photonic crystal fibers. *Optical Materials*, *32*(11), 1532-1539.

Dongol, M. (2002). Optical absorption and structural properties of as-deposited and thermally annealed As-Te-Ga thin films. *Egypt. J. Solids*, *25*(1), 33-47.

Eggleton, B. J., Luther-Davies, B., & Richardson, K. (2011). Chalcogenide photonics. *Nature photonics*, *5*(3), 141-148.

El-Metwally, E. G., Atyia, H. E., & Ismail, A. M. (2022). Impact of Se and Te addition on optical characteristics of ternary GeInSb chalcogenide films as promising materials for optoelectronic applications. Physica Scripta, 97(8), 085816.

El-Ocker, M. M., Fayek, S. A., Metawe, F., & Hassanien, A. S. (1998). Thermal Behaviour and Non-Isothermal Kinetics of Ge10+ xSe40Te50-x Amorphous System. *Indian Journal of Physics*.

Fayek, S. A., El-Ocker, M., & Hassanien, A. S. (2001). Optical and electrical properties of Ge10+ xSe40Te50− x thin film. *Journal of Materials Research*, *16*(6), 1549-1553.

Fouad, S. S., Amin, G. A. M., & El-Bana, M. S. (2018). Physical and optical characterizations of Ge10Se90− xTex thin films in view of their spectroscopic ellipsometry data. *Journal of Non-Crystalline Solids*, *481*, 314-320.

Giri, S., Priyadarshini, P., Alagarasan, D., Ganesan, R., & Naik, R. (2023). Annealing-induced phase transformation in In 10 Se 70 Te 20 thin films and its structural, optical and morphological changes for optoelectronic applications. RSC advances, 13(36), 24955-24972

Gopinath, J. T., Soljačić, M., Ippen, E. P., Fuflyigin, V. N., King, W. A., & Shurgalin, M. (2004). Third order nonlinearities in Ge-As-Se-based glasses for telecommunications applications. *Journal of Applied Physics*, *96*(11), 6931-6933.

Halenkovič, T., Baillieul, M., Gutwirth, J., Němec, P., & Nazabal, V. (2022). Amorphous Ge-Sb-Se-Te chalcogenide films fabrication for potential environmental sensing and nonlinear photonics. Journal of Materiomics, 8(5), 1009-1019.

Hassanien, A. S. (2016). Studies on dielectric properties, opto-electrical parameters and electronic polarizability of thermally evaporated amorphous Cd50S50− xSex thin films. *Journal of Alloys and Compounds*, *671*, 566-578.

Hassanien, A. S., & Akl, A. A. (2016). Effect of Se addition on optical and electrical properties of chalcogenide CdSSe thin films. *Superlattices and Microstructures*, *89*, 153-169.

Hassanien, A. S., & Akl, A. A. (2016). Electrical transport properties and Mott's parameters of chalcogenide cadmium sulphoselenide bulk glasses. *Journal of Non-Crystalline Solids*, *432*, 471-479.

Hassanien, A. S., & Akl, A. A. (2018). Influence of thermal and compositional variations on conduction mechanisms and localized state density of amorphous Cd50S50− xSex thin films. *Journal of Non-Crystalline Solids*, *487*, 28-36.

Hassanien, A. S., & Akl, A. A. (2018). X-ray studies: CO 2 pulsed laser annealing effects on the crystallographic properties, microstructures and crystal defects of vacuum-deposited nanocrystalline ZnSe thin films. *CrystEngComm*, *20*(44), 7120-7129.

Hassanien, A. S., & Sharma, I. (2019). Band-gap engineering, conduction and valence band positions of thermally evaporated amorphous Ge15-x Sbx Se50 Te35 thin films: Influences of Sb upon some optical characterizations and physical parameters. *Journal of Alloys and compounds*, *798*, 750-763.

Hassanien, A. S., & Sharma, I. (2020). Optical properties of quaternary a-Ge15-x Sbx Se50 Te35 thermally evaporated thin-films: refractive index dispersion and single oscillator parameters. *Optik*, *200*, 163415.

Hassanien, A. S., Aly, K. A., & Akl, A. A. (2016). Study of optical properties of thermally evaporated ZnSe thin films annealed at different pulsed laser powers. *Journal of Alloys and Compounds*, *685*, 733-742.

Jenkins, F. A., & White, H. E. (1957). Fundamentals of optics. *Indian Journal of Physics*, *25*, 265-266.

Jung, G. H., Kong, H., Yeo, J. B., Lee, H. Y., Jung, G. H., Kong, H., ... & Lee, H. Y. (2017). Evaluations of Sb 20 Se 80-x Ge x (x= 10, 15, 20, and 25) Glass Stability from Thermal, Structural and Optical Properties for IR Lens Application. *Journal of the Korean Ceramic Society*, *54*(6), 484-491.

Kastner, M., Adler, D., & Fritzsche, H. (1976). Valence-alternation model for localized gap states in lone-pair semiconductors. *Physical Review Letters*, *37*(22), 1504.

Krbal, M., Wagner, T., Vlcek, M., Vlcek, M., & Frumar, M. (2006). Optical properties and structure of amorphous films Agx (As0. 33S0. 67− ySey) 100− x. *Journal of non-crystalline solids*, *352*(23-25), 2662-2666.

Kumar, P., Kaur, J., Tripathi, S. K., & Sharma, I. (2017). Effect of antimony (Sb) addition on the linear and non-linear optical properties of amorphous Ge–Te–Sb thin films. *Indian Journal of Physics*, *91*, 1503-1511.

Kumar, P., Tripathi, S. K., & Sharma, I. (2018). Effect of Bi addition on the physical and optical properties of Ge20Te74-xSb6Bix (x= 2, 4, 6, 8, 10) thin films deposited via thermal evaporation. *Journal of Alloys and Compounds*, *755*, 108-113.

Kumar, V., & Dwivedi, D. K. (2013). Study on structural, optical and electrical properties of CdS0. 5Se0. 5 thin films for photovoltaic applications. *Optik*, *124*(16), 2345-2348.

Manifacier, J. C., Gasiot, J., & Fillard, J. P. (1976). A simple method for the determination of the optical constants n, k and the thickness of a weakly absorbing thin film. *Journal of Physics E: Scientific Instruments*, *9*(11), 1002.

Mishra, S., Lohia, P., & Dwivedi, D. K. (2019). Structural and optical properties of (Ge11. 5 Se67. 5 Te12. 5) 100− x Sbx (0≤ x≤ 30) chalcogenide glasses: A material for IR devices. *Infrared Physics & Technology*, *100*, 109-116.

Moss, T. S. (1985). Relations between the refractive index and energy gap of semiconductors. *physica status solidi (b)*, *131*(2), 415-427.

Pandey, V., Mehta, N., Tripathi, S. K., & Kumar, A. (2005). Optical band gap and optical constants in Se85Te15-xPbx thin films. *J. Optoelectron. Adv. Mater.*, *7*(5), 2641-2646.

Petit, L., Carlie, N., Chen, H., Gaylord, S., Massera, J., Boudebs, G., ... & Richardson, K. (2009). Compositional dependence of the nonlinear refractive index of new germanium-based chalcogenide glasses. *Journal of Solid State Chemistry*, *182*(10), 2756-2761.

Sati, D. C., Kumar, R., & Mehra, R. M. (2006). Influence of Thickness on Optical Properties of a: As_2Se_3 Thin Films. *Turkish Journal of Physics*, *30*(6), 519-528.

Shaaban, E. R., Ismail, Y. A., & Hassan, H. S. (2013). Compositional dependence of the optical properties of amorphous Se80− xTe20Bix thin films using transmittance and reflectance measurements. *Journal of non-crystalline solids*, *376*, 61-67.

Shaaban, E. R., Mahasen, M. M., Soraya, M. M., Yousef, E. S., Mahmoud, S. A., Ali, G. A., & Elshaikh, H. A. (2019). Dilute magnetic semiconductor of ZnCoSe thin films: Structural, optical, and magnetic characteristics. *Journal of the American Ceramic Society*, *102*(7), 4067-4081.

Shaaban, E. R., Yahia, I. S., Afify, N., Salem, G. F., & Dobrowolski, W. (2014). Structural and the optical dispersion parameters of nano-CdTe thin film/flexible substrate. *Materials science in semiconductor processing*, *19*, 107-113.

Sharma .I, S.K. Tripathi, P.B. Barman, J. Appl. Phys. 110 (2011) 043108-7..

Sharma, I., Kumar, P., & Tripathi, S. K. (2017). Physical and optical properties of bulk and thin films of a–Ge–Sb–Te lone-pair semiconductors. *Phase Transitions*, *90*(7), 653-671.

Sharma, N., Sharda, S., Sharma, V., & Sharma, P. (2013). Far-infrared investigation of ternary Ge–Se–Sb and quaternary Ge–Se–Sb–Te chalcogenide glasses. *Journal of non-crystalline solids*, *375*, 114-118.

Sharma, P., & Katyal, S. C. (2010). Linear and nonlinear refractive index of As–Se–Ge and Bi doped As–Se–Ge thin films. *Journal of Applied Physics*, *107*(11).

Soraya, M. M., Abdel-Wahab, F., Elamin, A. A., Shaaban, E. R., & Ali Karrar, N. N. (2023). Structural and thermal characteristics of Ge30− xSbxTe10Se60 (0≤ x≤ 20) glasses for electronic devices. *Journal of Thermal Analysis and Calorimetry*, 1-16.

Swanepoel, R. (1983). Determination of the thickness and optical constants of amorphous silicon. *Journal of Physics E: Scientific Instruments*, *16*(12), 1214.

Tanaka, K. (1980). Optical properties and photoinduced changes in amorphous As瑕 S films. *Thin solid films*, *66*(3), 271-279.

Tauc, J. (Ed.). (2012). *Amorphous and liquid semiconductors*. Springer Science & Business Media.

Ticha, H., & Tichy, L. (2002). Semiempirical relation between non-linear susceptibility (refractive index), linear refractive index and optical gap and its application to amorphous chalcogenides. *J. Optoelectron. Adv. Mater*, *4*(2), 381-386.

Urbach, F. (1953). The long-wavelength edge of photographic sensitivity and of the electronic absorption of solids. *Physical review*, *92*(5), 1324.

Vahalova, R., Tichý, L., Vlček, M., & Ticha, H. (2000). Far infrared spectra and bonding arrangement in some Ge–Sb–S glasses. *physica status solidi (a)*, *181*(1), 199-209.

Wang, C. C. (1970). Empirical relation between the linear and the third-order nonlinear optical susceptibilities. *Physical Review B*, *2*(6), 2045.

Wang, G., Nie, Q., Wang, X., Shen, X., Chen, F., Xu, T., ... & Zhang, X. (2011). New far-infrared transmitting Te-based chalcogenide glasses. Journal of Applied Physics, 110(4).

Wemple, S. H., & DiDomenico Jr, M. (1971). Behavior of the electronic dielectric constant in covalent and ionic materials. *Physical Review B*, *3*(4), 1338.

Yoo, S., Yoo, C., Park, E. S., Kim, W., Lee, Y. K., & Hwang, C. S. (2018). Chemical interactions in the atomic layer deposition of Ge–Sb–Se–Te films and their ovonic threshold switching behavior. *Journal of Materials Chemistry C*, *6*(18), 5025-5032.